6 Transducer Characterization

The sending and receiving transducers are some of the most important parts of an ultrasonic measurement system and also some of the most challenging components to completely characterize. To date there is no practical way to determine the complete transfer matrix components of a transducer, but as we have shown the role of the transducer as both a transmitter and a receiver in an ultrasonic measurement can be completely described in terms of its electrical impedance and sensitivity. In this Chapter we will describe methods to obtain a transducer's electrical impedance and sensitivity and also obtain a transducer's effective geometrical parameters such as effective radius and effective focal length.

6.1 Transducer Electrical Impedance

The transducer electrical impedance, $Z_{in}^{A;e}(\omega)$, of a given transducer A is relatively simple to determine in the calibration setup shown in Fig. 6.1. The transducer is connected by a short cable to the pulser and the input voltage, $v_1(t)$, and current, $i_1(t)$, are measured at point a as shown in Fig. 6.1 for the short time that the pulser is exciting the transducer and generating waves in the fluid but before any reflected waves have arrived back at the transducer. Taking the Fourier transform of these measurements to obtain $V_1(\omega), I_1(\omega)$ then gives the impedance directly since for a short cable the transfer matrix of the cable is just the unit matrix and $V_1(\omega) = V_{in}(\omega)$, $I_1(\omega) = I_{in}(\omega)$, where $V_{in}(\omega), I_{in}(\omega)$ are the voltage and current directly at the transducer electrical input port (point b in Fig. 6.1) and

$$Z_{in}^{A;e}(\omega) = \frac{V_{in}(\omega)}{I_{in}(\omega)}. \tag{6.1}$$

As discussed earlier for other measurements of this type, in implementing Eq. (6.1) it may be necessary to use a Wiener filter to desensitize the division

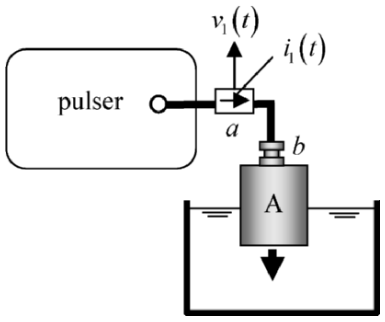

Fig. 6.1. A calibration setup for measurement of a transducer's electrical impedance.

process to noise (see Appendix C). The voltage measurement can be made by inserting a T-connector in the cable and measuring the voltage on the connector while the current can be measured directly by tapping the cable and using a commercial current probe (Tektronix CT-2, Tektronix, Inc., Wilsonville, OR) attached to the central conductor of the cable. A current probe of this type is shown in Fig. 6.2. If it is not practical to use a very short cable, then the measurements at point *a* must be compensated for cabling effects. This is easy to do since in this case

$$\begin{Bmatrix} V_{in} \\ I_{in} \end{Bmatrix} = \frac{1}{\det[\mathbf{T}]} \begin{bmatrix} T_{22} & -T_{12} \\ -T_{21} & T_{11} \end{bmatrix} \begin{Bmatrix} V_1 \\ I_1 \end{Bmatrix}, \tag{6.2}$$

where $[\mathbf{T}]$ is the transfer matrix for the cable between points *a* and *b* in Fig. 6.1 (considering *a* as the input port and *b* the output port). If the cabling acted as an ideal reciprocal device the determinant of the transfer matrix would be unity, i.e. $\det[\mathbf{T}] = 1$. In practice, the measured determinant is normally close to but not identically unity so those small differences are accounted for by using Eq. (6.2) with the determinant calculated directly from the measured component values. If the cable transfer matrix has been measured, we can use Eq. (6.2) to determine $V_{in}(\omega), I_{in}(\omega)$ from $V_1(\omega), I_1(\omega)$ and use Eq. (6.1) to obtain the impedance.

Figure 6.3 shows a measured transducer impedance plotted versus the frequency, *f*. To first order the magnitude of the impedance varies like 1/*f* and the phase is approximately 90 degrees. Figure 6.4 shows the corresponding frequency response of a capacitor, which we see has the

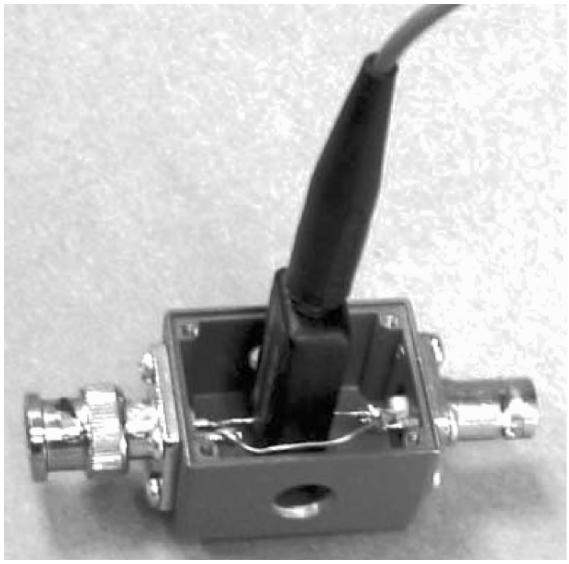

Fig. 6.2. A probe for measuring the current in a cable.

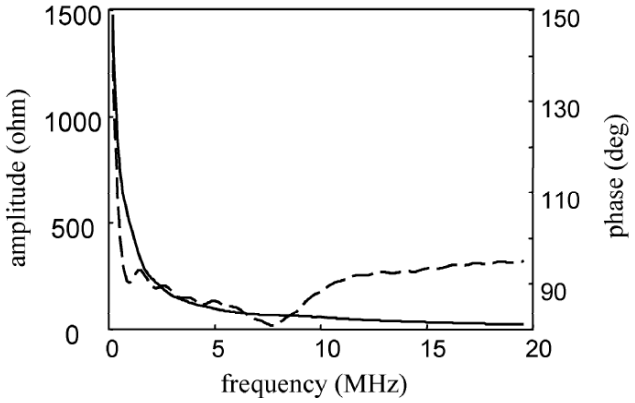

Fig. 6.3. The measured electrical impedance of a transducer showing the magnitude of the impedance (solid line) and the phase (dashed line) versus frequency.

same overall behavior. This is not surprising since a piezoelectric crystal that is plated on its faces will act to first order much like an ordinary capacitor. We cannot always expect to see purely a capacitor-like behavior

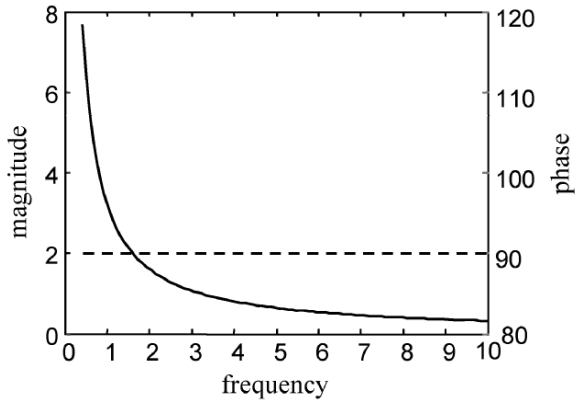

Fig. 6.4. The magnitude (solid line) and phase (dashed line) of the impedance, $Z^e = 1/(-2\pi i f C)$, of a capacitor versus frequency, f, where C is the capacitance.

for the impedance, however, if a commercial transducer contains additional internal electrical "tuning" elements.

6.2 Transducer Sensitivity

With a new pulse-echo technique that has been recently developed, determining the transducer sensitivity of transducer A, $S_{vI}^{A}(\omega)$, is only slightly more involved than finding the impedance [6.1]. In this case we use a calibration setup such as the one shown in both Figs. 6.5 and 6.6 where the waves from the transducer are reflected from a solid block at normal incidence and the acoustic/elastic transfer function, $t_A(\omega)$, is known (see Eq. (5.18)). We first measure the input voltage, $v_1(t)$, and current, $i_1(t)$, when the transducer is firing and before any reflected waves arrive at the transducer (Fig. 6.5). After a time delay of approximately $t = 2D/c_{p1}$, where c_{p1} is the wave speed in the water, we measure the received voltage, $v_2(t)$, and current, $i_2(t)$ generated by the waves reflected from the block (Fig. 6.6). In Fig. 6.7 we show the sound generation process model corresponding to Fig. 6.5, where the frequency components of $v_1(t), i_1(t)$ at point a are labeled $V_1(\omega), I_1(\omega)$ and the

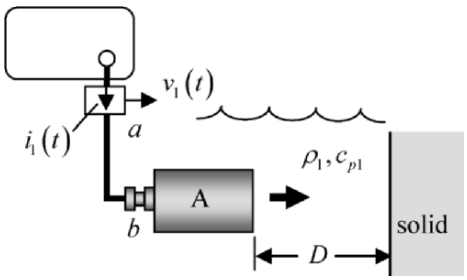

Fig. 6.5. Measurement of voltage and current when transducer *A* is radiating waves.

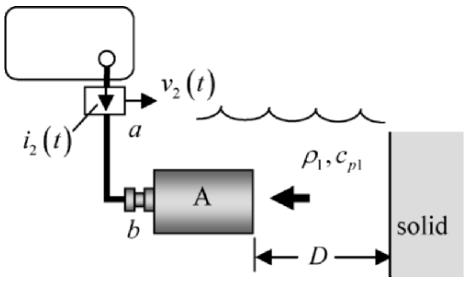

Fig. 6.6. Measurement of voltage and current when transducer *A* is receiving the waves reflected from the block.

frequency components of the voltage and current at the electrical input port are labeled $V_{in}(\omega), I_{in}(\omega)$. It is likely that the measurements of $v_1(t), i_1(t)$ must by physical necessity be made outside the water tank so that there may be a non-negligible length of cable between the measurement point *a* and the electrical port of the transducer (point *b*). Again, however, if the transfer matrix [**T**] of the cabling is known, the voltages and currents measured in these two setups can be related directly to the corresponding voltages and currents at the transducer electrical input port. During the sound generation process, we can again use Eq. (6.2). Note that $V_{in}(\omega)$ and $I_{in}(\omega)$ here are identical to those used in Eq. (6.1) so

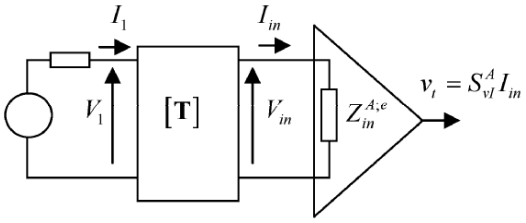

Fig. 6.7. The generation process model for the measurement of voltage and current when transducer A radiates waves.

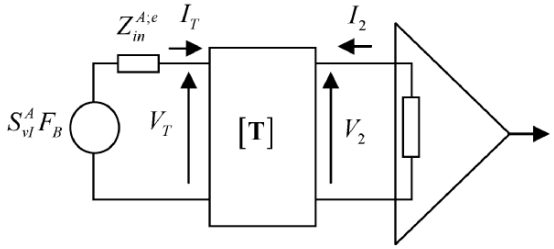

Fig. 6.8. The reception process model for the measurement of the voltage and current when transducer A receives waves reflected from the block.

that the impedance can also be calculated directly in the setup of Fig. 6.5 from $Z_{in}^{A;e}(\omega) = V_{in}(\omega)/I_{in}(\omega)$. In Fig. 6.8 we show the sound reception process model corresponding to Fig. 6.6 where the frequency components of $v_2(t), i_2(t)$ at point *a* are labeled $V_2(\omega), I_2(\omega)$ and the frequency components of the voltage and current at the electrical input port are labeled $V_T(\omega), I_T(\omega)$. To compensate for the cabling in this case we note that $(V_T, -I_T)$ in the reception process (Fig. 6.8) replaces (V_{in}, I_{in}) in the generation process (Fig. 6.7) and similarly (V_2, I_2) replaces (V_1, I_1) so we find

$$\begin{Bmatrix} V_T \\ -I_T \end{Bmatrix} = \frac{1}{\det[\mathbf{T}]} \begin{bmatrix} T_{22} & -T_{12} \\ -T_{21} & T_{11} \end{bmatrix} \begin{Bmatrix} V_2 \\ I_2 \end{Bmatrix}. \tag{6.3}$$

Note that I_1 and I_2 are taken to be in the same direction in both cases since these currents are both measured by the current probe in Fig. 6.2.

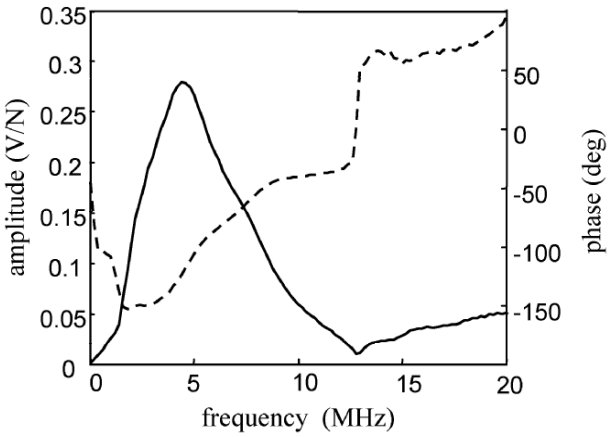

Fig. 6.9. The measured sensitivity of a 5MHz, 6.35 mm radius planar transducer. The magnitude of the sensitivity versus frequency (solid line) and phase versus frequency (dashed line).

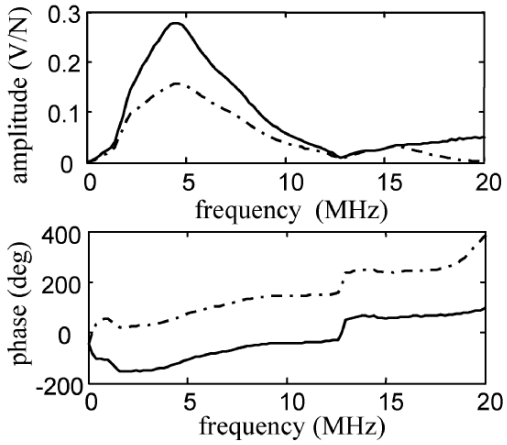

Fig. 6.10. The measured sensitivity of a transducer as determined with compensation for cabling effects (solid line) and where cabling effects are ignored (dash-dot line).

This probe is directional and is oriented so that it measures the current flowing into the cable at point *a* during both the sound generation and reception processes (see Figs. 6.5 and 6.6).

Now, consider determining the sensitivity from these measurements. From Fig. 6.8 we have

$$S_{vI}^{A} F_B = Z_{in}^{A;e} I_T + V_T \tag{6.4}$$

and also

$$\begin{aligned} F_B &= \frac{F_B}{F_t}\frac{F_t}{v_t}\frac{v_t}{I_{in}} I_{in} \\ &= t_A Z_r^{A;a} S_{vI}^{A} I_{in} \end{aligned} \tag{6.5}$$

so that by combining these two relations and using $Z_{in}^{A;e} = V_{in} / I_{in}$ we obtain

$$S_{vI}^{A} = \sqrt{\frac{V_{in} I_T + V_T I_{in}}{t_A Z_r^{A;a} I_{in}^2}}. \tag{6.6}$$

Since we know the acoustic/elastic transfer function for this setup and we can take the acoustic radiation impedance as its high frequency value $Z_r^{A;a} = \rho_1 c_{p1} S_A$, measurements of $V_{in}(\omega), I_{in}(\omega), V_T(\omega), I_T(\omega)$ are sufficient to determine the transducer sensitivity. Since Eq. (6.6) involves division of frequency domain values, a Wiener filter can be used here also to handle noise issues.

Figure 6.9 shows a plot of a measured sensitivity. The dimensions of the sending sensitivity S_{vI}^{A} are velocity/current while the open-circuit receiving sensitivity, $M_{VF_B}^{A;\infty}$, has the dimensions of voltage/force. Since these two sensitivities are equal we can use either set of dimensions. We choose here to use Volts/Newton in the SI system to characterize these sensitivities. Figure 6.10 shows the differences in the measured sensitivity obtained when cabling effects are accounted for and when they are ignored. In most immersion setups such as the one used here there will likely be more than a meter of cable between where the voltages and currents are measured and the transducer electrical port, so that the cabling effects cannot be ignored, as shown in Fig. 6.10. It is important to realize that when the measured signals and modeled parameters are combined they determine the square of the transducer sensitivity, not the sensitivity itself. This can be seen from Eq. (6.6) if we rewrite it as

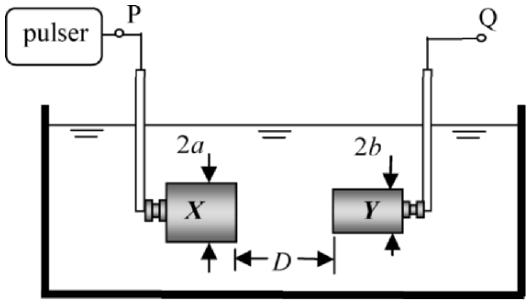

Fig. 6.11. A generic pitch-catch setup that can be used with three transducers (in various pairs) to determine the sensitivity of one of those transducers.

$$\left[S_{vI}^{A}(\omega)\right]^2 = \frac{V_{in}(\omega)I_T(\omega)+V_T(\omega)I_{in}(\omega)}{t_A(\omega)Z_r^{A;a}(\omega)I_{in}^2(\omega)} \tag{6.7}$$

Thus, when the square root is taken of these values there is always an ambiguity about the sign that should be chosen. In a pulse-echo experiment, the sign is immaterial in predicting the measured voltage output of the system since the output voltage is proportional to the sensitivity squared (same transducer is both sender and receiver). In a pitch-catch experiment, however, two different transducers are used and this ambiguity in sign could affect the polarity of the predicted output voltage. There is no way to resolve the sign with the procedures discussed here, but there are two ways to deal with this issue. In a pitch-catch situation, the measured sensitivities of the two transducers involved could be combined with measurements of the other system components to predict the system function $s(\omega)$. If the transducers were placed in a measurement setup where the acoustic/elastic transfer function, $t_A(\omega)$ was known (such as the setup shown in Fig. 5.4) then the output voltage, $V_R(\omega) = s(\omega)t_A(\omega)$ could be obtained and Fourier transformed into the time domain and compared to the experimentally observed signal. If the predicted polarity of the time domain signal was correct (i.e. agreed with the experimental voltage), one could say that the signs of the two sensitivities were consistent. If the polarities did not agree, one could change the sign on one of the sensitivities to make them consistent. To determine the sign in a more fundamental manner one could instead place

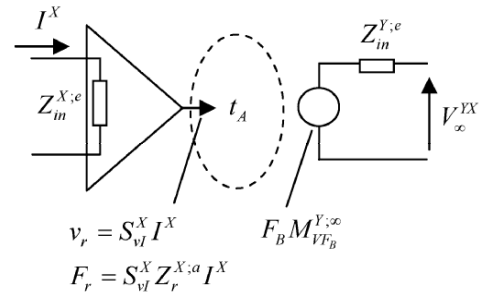

Fig. 6.12. A model for the generic pitch-catch setup of Fig. 6.11, showing the transmitting and receiving transducers and the acoustic/elastic transfer function that defines the wave processes occurring between them.

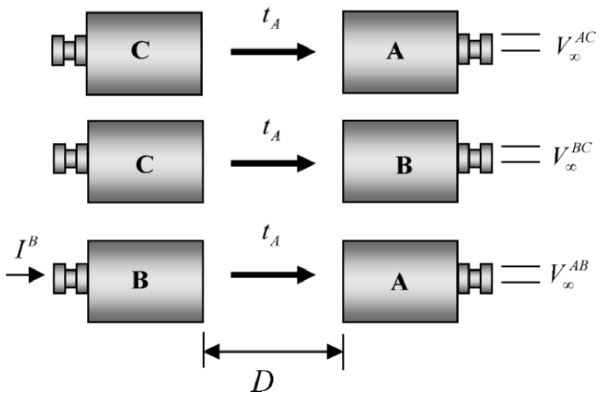

Fig. 6.13. Three separate pitch-catch setups and measurements for determining the sensitivity of transducer *A*. In this case we have assumed the transducers are all of the same diameter and the distance, *D*, is fixed for all three setups.

the transducer in a setup where the input current driving the transducer was measured as well as the pressure in the transducer wave field (such as the on-axis pressure measured with a separate calibrated probe). Such a measurement setup would only be needed, however, if it was essential to predict in an absolute sense the generated pressure wave field.

There exists another reciprocity-based measurement procedure to determine the open-circuit receiving sensitivity, $M_{VF_B}^{A;\infty}$, that is commonly described in the acoustics literature [6.2-6.10]. That method requires one to make measurements with three different transducers in three separate pitch-catch setups of the generic type shown in Fig (6.11) where the

transmitting transducer is transducer X and the receiving transducer is transducer Y. The input current to transducer X measured at point P in Fig. 6.11 is labeled I^X and the open-circuit voltage measured at point Q received by transducer Y due to the waves generated by transducer X is labeled V_∞^{YX}. If the effects of cabling between point P and the transmitting transducer X and between transducer Y and point Q are both negligible, then the measured current at the input port of transducer X is the same as I^X and the open-circuit voltage at Q is the same as the open-circuit voltage directly at the receiving transducer electrical port. In this case the sound generation and reception model for the pitch-catch setup of Fig. 6.11 is as shown in Fig. 6.12, Note that the acoustic/elastic transfer function, t_A, for this pitch/catch configuration is known for a pair of circular, plane piston transducers (see Eq. (5.10) for the case where the transducers are of different size, or Eq. (5.12) when the transducers are of the same size). Since the open-circuit voltage at the receiving transducer electrical port is just the equivalent source term for transducer Y given by $F_B M_{VF_B}^{Y;\infty}$ (see Chapter 5) we find

$$\begin{aligned}\frac{V_\infty^{YX}}{I^X} &= \frac{F_B M_{VF_B}^{Y;\infty}}{I^X} \\ &= \frac{F_B}{F_t}\frac{F_t}{I^X} M_{VF_B}^{Y;\infty} \\ &= t_A Z_r^{X;a} S_{vI}^X M_{VF_B}^{Y;\infty}.\end{aligned} \tag{6.8}$$

As shown in Chapter 5 the transmitting sensitivity S_{vI}^Z and the open-circuit receiving sensitivity, $M_{VF_B}^{Z;\infty}$, are the same for any reciprocal transducer Z (where $Z = X$ or Y), so we can express the voltage over current ratio in Eq. (6.8) in terms of either of these sensitivities. We will choose the open-circuit receiving sensitivity here, as that is the choice normally made in the acoustics literature. Then Eq. (6.8) becomes

$$\frac{V_\infty^{YX}}{I^X} = t_A Z_r^{X;a} M_{VF_B}^{X;\infty} M_{VF_B}^{Y;\infty}. \tag{6.9}$$

Now, apply Eq.(6.9) to the three separate pitch-catch setups involving three transducers A, B, and C shown schematically in Fig. 6.13, where we have assumed that the distance, D, between transducers is held fixed for all three setups and the diameters of all three transducers are the same so that there is only one acoustic/elastic transfer function, t_A, for all three setups.

In setup one transducer $X = C$ is firing and transducer $Y = A$ is receiving while for setup two transducer $X = C$ again is firing and transducer $Y = B$ is receiving. In setup three, transducer $X = B$ is firing and transducer $Y = A$ is receiving. Applying Eq. (6.9) to each of these cases individually we have

$$\begin{aligned}
\frac{V_{\infty}^{AC}}{I^{C}} &= t_{A} Z_{r}^{C;a} M_{VF_B}^{A;\infty} M_{VF_B}^{C;\infty} \\
\frac{V_{\infty}^{BC}}{I^{C}} &= t_{A} Z_{r}^{C;a} M_{VF_B}^{B;\infty} M_{VF_B}^{C;\infty} \\
\frac{V_{\infty}^{AB}}{I^{B}} &= t_{A} Z_{r}^{B;a} M_{VF_B}^{A;\infty} M_{VF_B}^{B;\infty}.
\end{aligned} \tag{6.10}$$

From Eq. (6.10) we see we can eliminate the sensitivities of transducers B and C by considering the particular combination of ratios

$$\frac{\left(\frac{V_{\infty}^{AB}}{I^{B}}\frac{V_{\infty}^{AC}}{I^{C}}\right)}{\left(\frac{V_{\infty}^{BC}}{I^{C}}\right)} = t_{A} Z_{r}^{B;a}\left[M_{VF_B}^{A;\infty}\right]^{2} \tag{6.11}$$

so solving for the open-circuit receiving sensitivity of transducer A we find:

$$M_{VF_B}^{A;\infty} = S_{vI}^{A} = \sqrt{\frac{V_{\infty}^{AB} V_{\infty}^{AC}}{V_{\infty}^{BC} I^{B}} \frac{1}{Z_{r}^{B;a} t_{A}}}. \tag{6.12}$$

Equation (6.12), which is similar to the expression commonly found in the acoustics literature, is very much like Eq. (6.6) for our pulse-echo method. Instead of the two voltage and two current measurements needed for the pulse-echo method, Eq. (6.11) requires that we make three open-circuit voltage methods and one current measurement from the three pitch-catch setups of Fig. 6.13. For acoustic transducers operating at kHz frequencies or less, Eq. (6.12) has been commonly used in the acoustics community for many years to obtain transducer sensitivity. In fact, for transducers at those frequencies there exists a commercially available calibration system that can implement the measurements required in Eq.(6.12) and extract the sensitivity [6.11]. Dang. et al. [6.12] have also used this three transducer method to obtain the sensitivity of NDE transducers operating at MHz frequencies. However, Dang et al. [6.12] found that at MHz frequencies it was important to consider the effects of the cabling present. They defined a

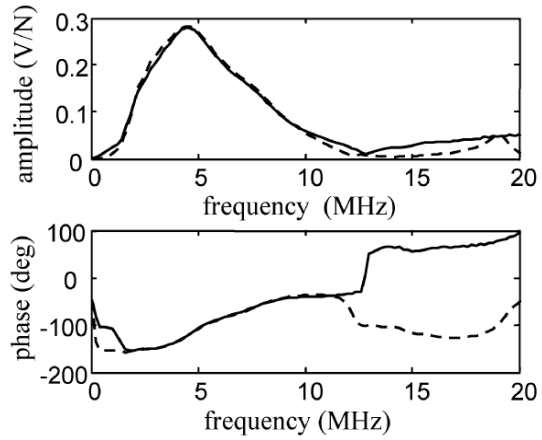

Fig. 6.14. The magnitude and phase of the sensitivity, S_{vI} , of a 5 MHz, 6.35 mm diameter planar transducer as calculated by the pulse-echo method (solid line) and the three transducer pitch-catch method (dashed line).

generalized sensitivity that took into account those cable effects and applied a modified version of Eq. (6.12).

The three transducer pitch-catch method is also a viable approach to obtaining sensitivity but the pulse-echo method has several advantages. First, the three-transducer method requires one to make measurements in three separate pitch-catch setups while only one setup is needed in the pulse-echo method. This makes the pulse-echo method faster and avoids any delicate re-alignment issues for the transducers. Second, we note that both the pulse-echo and the three transducer pitch-catch procedure for obtaining sensitivity are model-based approaches. This means that the model assumptions made on transducer behavior must be satisfied for all three transducers for the three transducer method but only for the transducer whose sensitivity is to be determined for the pulse-echo method. Figure 6.14 shows the sensitivity of a 5 MHz, 6.35 mm diameter planar transducer obtained via either the pulse-echo method or the three-transducer pitch-catch method. It can be seen that there is little difference between the results obtain with either method over the bandwidth of the transducer.

There is also a pulse-echo technique for determining sensitivity called the self-reciprocity method that has been developed in the acoustics literature [6.13-6.17]. The self-reciprocity method applies Eq. (6.9) to a

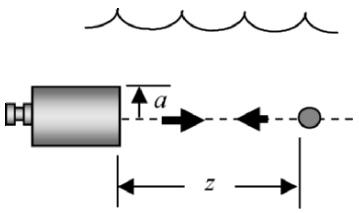

Fig. 6.15. A circular piston transducer of radius *a* receiving the waves reflected from the front surface of a spherical reflector located on the central axis of the transducer.

pulse-echo setup involving a single transducer, A, and solves for the sensitivity of A in the form

$$M_{VF_B}^{A;\infty} = S_{vI}^{A} = \sqrt{\frac{V_{\infty}^{AA}}{I^{A}} \frac{1}{t_A Z_r^{A;a}}}, \tag{6.13}$$

where V_{∞}^{AA} is the open-circuit voltage received by A due to the waves generated by A and I^{A} is the current driving transducer A when it is radiating into the fluid. Equation (6.13) is very similar to our pulse-echo expression, Eq. (6.6). In fact under open-circuit conditions $I_T = 0$ in Eq. (6.6) and that equation simply reduces to Eq. (6.13). However, in order to apply Eq. (6.13) directly one needs to measure the received voltage under open-circuit conditions. Since inherently in a pulse-echo setup the transducer will be loaded by the receiver and cabling on reception, this has forced some authors to use rather complicated measurement systems or special matching networks to infer the open-circuit response. Equation (6.6) can be applied directly from measurements taken under the actual conditions present in a pulse-echo setup, so it is significantly more convenient to use than Eq. (6.13).

6.3 Transducer Effective Radius and Focal Length

It would appear that geometrical parameters such as the transducer radius and focal length are parameters that are well-defined and need no experimental determination. In practice, however, it has been found that if one simply uses these parameters (as specified by the transducer manufacturer)

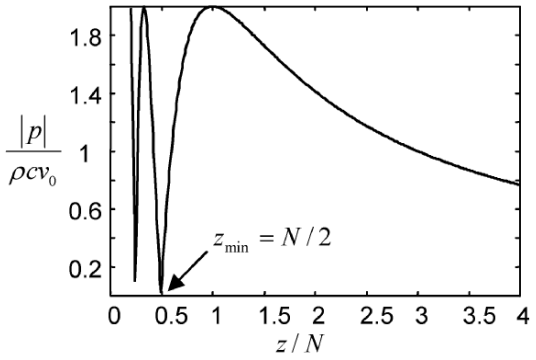

Fig. 6.16. The magnitude of the on-axis normalized pressure versus normalized distance z/N for a ½ inch diameter circular piston transducer radiating waves at 5 MHz into a fluid, where N is the near field distance given by $N = a^2/\lambda$. As shown the last on-axis null occurs at one-half a near field distance.

in transducer beam models, one often does not get good agreement with theory when the behavior of the transducer beam is examined experimentally [6.18], [Fundamentals]. This is perhaps to be expected since, for example, a transducer crystal cannot have piston-like behavior over its entire face as the crystal is supported and constrained at its edges. Thus, one might define an *effective radius* for the transducer where a piston model agrees better with experiments. Similarly, the geometrical focal length of a focused transducer is determined in reality by a number of other unknown parameters such as the material properties and geometry of the focusing lens. Again, one might deal with these unknowns by defining an *effective focal length* that matches experiments.

First, consider the problem of determining the effective radius of a circular, planar immersion transducer. One configuration that can be used to determine the effective radius of this transducer is shown in Fig. 6.15. A spherical reflector is placed on the axis of the transducer and the transducer is scanned so that the sphere remains on the transducer's central axis at different distances, z. At each value of z, $z = z_i$ the received time domain voltage response, $v_R(t, z_i)$, from the front surface of the sphere is recorded and Fourier transformed to obtain its spectrum, $V_R(f, z_i)$. Then the magnitude of these frequency domain responses are plotted versus z at a single fixed frequency, f_0, which is usually taken near the center frequency of the transducer. Since the front surface reflection from the

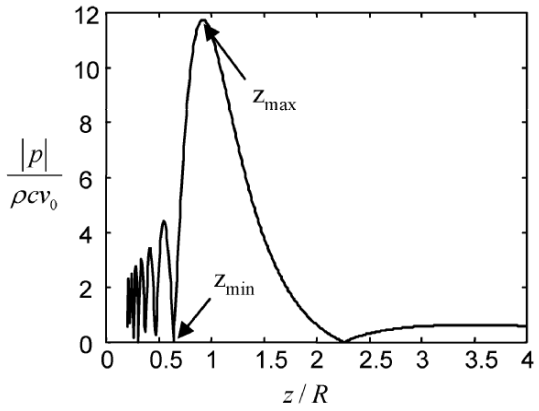

Fig. 6.17. The magnitude of the normalized on-axis pressure versus normalized distance z/R for a spherically focused piston transducer of radius a and geometrical focal length, R, radiating into water. The location of the null and maximum that are used in the determination of the effective focal length and radius are shown.

sphere is proportional to the square of the on-axis pressure of the transducer, the magnitude of the frequency domain plot of $V_R(f_0, z_i)$ has the same behavior as the on-axis pressure squared of the transducer when it is driven harmonically at frequency f_0 [Fundamentals]. In Chapter 8, an explicit expression for the on-axis pressure of a circular plane piston transducer at a fixed frequency is obtained analytically. This on-axis pressure is plotted in Fig. 6.16 versus the non-dimensional distance z/N, where $N = a^2/\lambda$ is called the near field distance and $\lambda = c_p / f_0$ is the wave length. It can be seen that in the region near the transducer there are a series of maxima and nulls. The last null (the one farthest from the transducer) can be shown to be located at the distance $z_{\min} = a^2/2\lambda$. Since this is a null of the pressure field the squared pressure will also have a null at this position, as will $|V_R(f_0, z_i)|$. If, from the plot of $|V_R(f_0, z_i)|$ versus z one obtains an estimate of the distance to that null then one can define the corresponding effective radius, a_{eff}, as

$$a_{eff} = \sqrt{2\lambda z_{\min}}. \tag{6.14}$$

This last on-axis null position is used because it is relatively simple to determine experimentally and does not require knowledge of the absolute amplitude of the on-axis pressure wave field. Some authors have used multiple on-axis nulls to obtain a better estimate of the effective radius or have used a least squares fitting to theory of many points, both on- and off-axis, in the transducer wave field to determine a_{eff}. All of these methods have the same goal – namely to obtain an estimate of a radius value that will match the theoretical wave field better than simply using the nominal radius. In principle the determination of a_{eff} in this fashion can be done at any fixed frequency and the result should not depend on the frequency chosen. In practice some variations of the effective radius value with frequency are found [Fundamentals]. Often these variations are not severe and a simple averaging of a_{eff} values over the bandwidth of the transducer gives good results.

For a spherically focused transducer one can use the same setup shown in Fig. 6.15 and the same procedures to obtain $\left|V_R\left(f_0, z_i\right)\right|$, which is proportional to the on-axis pressure squared wave field, but in this case we must obtain estimates of both the effective radius, a_{eff}, and the effective geometrical focal length, R_{eff} [6.19], [6.20]. Figure 6.17 shows a plot of a model prediction of the on-axis pressure of a circular, spherically focused piston transducer radiating into water. Again one sees nulls and maxima in the region close to the transducer and a very large peaked response due to focusing. Only the distance, $z_{\min}$, to the last on-axis null can generally be obtained reliably, however, since at other nulls the response rapidly gets very small. One could also measure the distance, $z_{\max}$, to the maximum value of $\left|V_R\left(f_0, z_i\right)\right|$, which also occurs when the magnitude of the pressure is a maximum. In this case, models show that the effective focal length is given in terms of $z_{\min}$ and $z_{\max}$ by [Fundamentals]

$$R_{eff} = z_{\max}\left\{\frac{\pi - x}{\pi - x\left(z_{\max} / z_{\min}\right)}\right\}, \tag{6.15}$$

where x is a solution of the transcendental equation

$$x\cos\left(x\right) = \frac{\pi - x\left(z_{\max} / z_{\min}\right)}{\pi - x}\sin\left(x\right). \tag{6.16}$$

Once the effective focal length is found from these relations the effective radius is given by

$$a_{eff} = \sqrt{\frac{2\lambda z_{\min} R_{eff}}{R_{eff} - z_{\min}}}, \tag{6.17}$$

which we see reduces to the planar transducer case (Eq. (6.14)) when $R_{eff} \to \infty$. In practice it has been found that the location of the distance to the transducer peak response, $z_{\max}$, is difficult to determine precisely and the results for R_{eff} are sensitive to those errors. It has been found better to use a range of estimates for $z_{\max}$ and choose the best combination of R_{eff} and a_{eff} values that match (in a least squares sense) the predicted and measured on-axis pressure values around the transducer focus. The details of these procedures can be found in [6.20]. There are other fitting methods that can be used to obtain these effective parameters but we will not discuss those alternatives here. As in the planar case, the effective parameters have been found to depend somewhat on the frequency one chooses, so one might need to take an average of their values over the bandwidth of the transducer.

Table 6.1. Effective radii and focal lengths found for some commercial transducers.

Transducers	Manufacturer's Specs		Effective Parameters		Center Frequency (MHz)
	R (mm)	a (mm)	R_{eff} (mm)	a_{eff} (mm)	
A	76.2	4.76	134.7	4.51	10
B	76.2	6.35	207.4	5.56	5
C	76.2	4.76	74.5	4.69	15

Equation (6.15) shows that the effective geometrical focal length, R_{eff}, is always larger than $z_{\max}$. The distance $z_{\max}$, which is the distance to the maximum on axis pressure, is often called the location of the "true focus". The difference between R_{eff} and $z_{\max}$ occurs because of wave diffraction effects at finite frequencies. It is only in the limit when the frequency goes to infinity that $z_{\max} / z_{\min} \to 1$, and one finds $R_{eff} = z_{\max}$.

Table 6.1 gives some example values of the effective parameters obtained for several commercial transducers. It can be seen that in some

cases the effective values are considerably different from the nominal values given by the transducer manufacturer. Those differences can lead to large errors if the nominal values are used in model calculations.

6.4 References

6.1 Lopez-Sanchez A, Schmerr LW (2006) Determination of an ultrasonic transducer's sensitivity and impedance in a pulse-echo setup. IEEE Trans. Ultrason., Ferroelect., Freq. Contr. 53: 2101-2112

6.2 Bobber RJ (1960) Underwater electroacoustic measurements. Naval Research Laboratory, Washington, DC

6.3 MacLean WR (1940) Absolute measurement of sound without a primary standard. J. Acoust. Soc. Am. 12: 140-146

6.4 Cook RK (1941) Absolute pressure calibration of microphone. J. Acoust. Soc. Am. 12: 415-420

6.5 DiMattia AL, Wiener FM (1946) On the absolute pressure calibration of condenser microphones by the reciprocity method. J. Acoust. Soc. Am. 18: 341-344

6.6 Ebaugh P, Mueser RE (1947) The practical application of the reciprocity theorem in the calibration of underwater sound transducers. J. Acoust. Soc. Am. 19: 695-700

6.7 Wathen-Dunn W (1949) On the reciprocity free-field calibration of microphones. J. Acoust. Soc. Am. 21: 542-546

6.8 Diestel HG (1961) Reciprocity calibration of microphones in a diffuse sound field. J. Acoust. Soc. Am. 33: 514-518

6.9 Hill EK, Egle DM (1980) A reciprocity technique for estimating the diffuse-field sensitivity of piezoelectric transducers. J. Acoust. Soc. Am. 67: 666-672

6.10 Vorlander M, Bietz H (1994) Novel broad-band reciprocity technique for simultaneous free-field and diffuse-field microphone calibration. Acustica 80: 365-377

6.11 Product Data Sheet, Reciprocity Calibration System – Type 9699 – Brüel & Kjaer

6.12 Dang CJ, Schmerr LW, Sedov A (2002) Ultrasonic transducer sensitivity and model-based transducer characterization. Research in Nondestructive Evaluation 14: 203-228

6.13 Carstensen EL (1947) Self-reciprocity calibration of electroacoustic transducers. J. Acoust. Soc. Am. 19: 961-965

6.14 White RM (1957) Self-reciprocity transducer calibration in a solid medium. J. Acoust. Soc. Am. 29: 834-836

6.15 Reid JM (1974) Self-reciprocity calibration of echo-ranging transducers. J. Acoust. Soc. Am. 55: 862-868

6.16 Widener MW (1980) The measurement of transducer efficiency using self reciprocity techniques. J. Acoust. Soc. Am, 67: 1058-1060

6.17 Brendel K, Ludwig G (1976/77) Calibration of ultrasonic standard probe transducers. Acustica 36: 203-208
6.18 Chivers RC, Bosselaar L, Filmore PR (1980) Effective area to be used in diffraction correction. J. Acoust. Soc. Am. 68: 80-84
6.19 Amin F, Gray TA, Margetan FJ (1991) A new method to estimate the effective geometrical focal length and radius of ultrasonic focused probes. In: Thompson DO, Chimenti DE (eds) Review of progress in quantitative nondestructive evaluation, 10A. Plenum Press, New York, NY, pp 861-865
6.20 Lerch T, Schmerr LW (1996) Characterization of spherically focused transducers using an ultrasonic measurement model approach. Res. Nondestr. Eval. 8: 1-21

6.5 Exercises

1. The MATLAB function transducer_x(z) returns the time-domain sampled voltage received from a spherical reflector in water (c = 1480 m/sec) located at a distance z (in mm) along the axis of a planar transducer as shown in Fig. (6.15). There are 1024 samples in this waveform, each separated by a sampling time interval Δt =.01 μsec. First, let z be the vector of values:

```
>> z = linspace (25, 400, 100);
```

Use this set of values in the transducer_x function, i.e. evaluate

```
>> V = transducer_x(z);
```

The matrix V will contain 100 waveforms calculated at each of these z-values. Use FourierT to generate the frequency spectra of these waveforms. Note that FourierT can operate on all of these waveforms at once as long as they are in columns (which is the case) and will return a matrix of the corresponding spectra, also in columns. Examine the magnitude of some of these spectra versus frequency to determine the range of frequencies over which there is a significant response. Pick one frequency value near the center frequency in this range and plot the magnitude of the spectra at that value versus the distance z.

Locate the last on-axis minimum in this plot and use Eq. (6.14) to determine the effective radius of this transducer. Try using a different frequency value within the transducer bandwidth to determine the effective radius. Does your answer vary with the frequency chosen?